

Remote sensing of seasonal changes and disturbances in mangrove forest: a case study from South Florida

KEQI ZHANG,^{1,2,†} BINA THAPA,¹ MICHAEL ROSS,^{1,3} AND DANIEL GANN⁴

¹*Department of Earth and Environment, Florida International University, Miami, Florida 33199 USA*

²*International Hurricane Research Center, Florida International University, Miami, Florida 33199 USA*

³*Southeast Environmental Research Center, Florida International University, Miami, Florida 33199 USA*

⁴*GIS-Remote Sensing Center, Florida International University, Miami, Florida 33199 USA*

Citation: Zhang, K., B. Thapa, M. Ross, and D. Gann. 2016. Remote sensing of seasonal changes and disturbances in mangrove forest: a case study from South Florida. *Ecosphere* 7(6):e01366. 10.1002/ecs2.1366

Abstract. Knowledge of the spatial and temporal changes caused by episodic disturbances and seasonal variability is essential for understanding the dynamics of mangrove forests at the landscape scale, and for building a baseline that allows detection of the effects of future environmental change. In combination with LiDAR data, we calculated four vegetation indices from 150 Landsat TM images from 1985 to 2011 in order to detect seasonal changes and distinguish them from disturbances due to hurricanes and chilling events in a mangrove-dominated coastal landscape. We found that normalized difference moisture index (NDMI) performed best in identifying both seasonal and event-driven episodic changes. Mangrove responses to chilling and hurricane events exhibited distinct spatial patterns. Severe damage from intense chilling events was concentrated in the interior dwarf and transition mangrove forests with tree heights less than 4 m, while severe damage from intense hurricanes was limited to the mangrove forest near the coast, where tree heights were more than 4 m. It took 4–7 months for damage from intense chilling events and hurricanes to reach their full extent, and took 2–6 yr for the mangrove forest to recover from these disturbances. There was no significant trend in the vegetation changes represented by NDMI over the 27-yr period, but seasonal signals from both dwarf and fringe mangrove forests were discernible. Only severe damage from hurricanes and intense chilling events could be detected in Landsat images, while damage from weak chilling events could not be separated from the background seasonal change.

Key words: chilling event; disturbance; freeze; hurricane; Landsat; LiDAR; mangrove; NDMI; NDVI; seasonal change; South Florida; Special Feature: Extreme Cold Spells; vegetation index.

Received 1 August 2015; revised 28 January 2016; accepted 10 February 2016. Corresponding Editor: E. Gaiser.

Copyright: © 2016 Zhang et al. This is an open access article under the terms of the Creative Commons Attribution License, which permits use, distribution and reproduction in any medium, provided the original work is properly cited.

† **E-mail:** zhangk@fiu.edu

INTRODUCTION

Mangroves are not only one of the most productive forest ecosystems but are also ideal for monitoring biological response to global climate change (Saintilan et al. 2014, Spalding et al. 2014). Mangroves have been experiencing significant changes worldwide due to sea level

rise, escalation in atmospheric CO₂ concentration, global surface temperature increase, and human development of coastal areas. Ross et al. (2000) and Krauss et al. (2014) demonstrated that the mangrove zone in South Florida has expanded landward and encroached into adjacent salt marsh zones due to sea level rise. Saintilan et al. (2014) showed poleward mangrove expansion

in response to climatic warming. In addition to these gradual changes, mangroves have been altered by episodic disturbances from hurricanes, freezes, or lightning strikes (Lugo and Patterson-Zucca 1977, Smith et al. 1994, Sherman et al. 2001, Stevens et al. 2006, Zhang 2008, Cavanaugh et al. 2014, Thapa 2014) that are more evident at the landscape scale, though they may contribute to or interact with global change factors that influence broader distributional trends. Mangrove trees can be killed, broken, and defoliated by the forces of high wind, storm surge, low temperature, or lightning, resulting in severe damage at scales ranging from the 10–20 m gap created by a lightning strike to the 50-km swath of tree death left in the wake of a hurricane eyewall's passage (Doyle et al. 1995, Zhang et al. 2008). Changes in the frequency or severity of these recurring events may have more immediate ecological impact on forest structure and composition than gradual changes in climate, acting powerfully to create patchiness and heterogeneity in a mangrove vegetation assemblage that in the New World is dominated by just a handful of tree species (White and Jentsch 2001). Therefore, it is important to document both episodic and gradual changes experienced by mangrove forests in order to understand coastal forest dynamics at the landscape level.

The phenology of mangrove trees responds to seasonal cycles in temperature, rainfall, and the supply of nutrients and fresh water. Leaf fall, flowering, and fruiting of mangroves exhibit seasonal patterns along the coast of Australia, at sites in Papua New Guinea and New Zealand, and in the subtropical region of Japan, although the timing of the annual peaks varies with the latitude of the sample sites (Duke 1990, Clarke 1994, Kamruzzaman et al. 2013). A recent study of the mangroves of Everglades National Park, USA, conducted over an 11-month period, suggested a seasonal fluctuation in spectral reflectance (Lagomasino et al. 2014). The spectral pattern, which was most prominent in near-infrared (NIR) wavelengths, seemed to coincide with seasonal variation in hydrological and nutrient conditions. Like disturbance events, within-year patterns in leaf area or plant function vary across the coastal landscape, but their spatial and temporal dimensions are rarely considered in tandem. Analyses of forest dynamics that incorporate both seasonal variation and fluctuations caused by episodic

events are needed in order to establish baseline understanding, i.e., a backdrop against which the effects of future global changes may be detected.

Most previous studies on seasonal and episodic changes have been based on repeated field surveys, with uncertain upscaling to the landscape level. More recently, advances in remote sensing technology and increases in the availability of long-term remotely sensed data (Wang and Xu 2010, Wang et al. 2010, Negrón-Juárez et al. 2014) have made assessment of landscape scale impacts of natural disturbances and seasonal changes more effective. However, most remote sensing studies of mangrove forests have focused on mapping changes in the distributions of species or forest types (Wang et al. 2004, Giri et al. 2011, Kuenzer et al. 2011), while only a few addressed the effects of disturbance (Zhang et al. 2008, Thapa 2014). Furthermore, none of these studies incorporated seasonal variation, or the effects of disturbances that differ as much in scale as hurricanes and chilling events.

The mangrove forests of southern Biscayne Bay, which experience seasonal changes, hurricanes, and chilling events, provide a unique opportunity to understand the role of natural disturbances in landscape dynamics. In this paper, we explore a remote sensing method capable of documenting these dynamics in a coastal landscape using Landsat imagery from 1985 to 2011. Our objectives are to (1) quantify the seasonal and episodic changes in mangrove forests, estimate their recovery rates following disturbances, and document any long-term trends; (2) characterize the spatial distribution of the disturbances from hurricanes and chilling events, and assess the relationship between disturbance and mangrove canopy height using light detection and ranging (LiDAR) data in combination with Landsat images; (3) determine the optimal vegetation index for detecting mangrove changes by comparing normalized difference vegetation index (NDVI), normalized difference moisture index (NDMI), soil adjusted vegetation index (SAVI) and enhanced vegetation index (EVI).

STUDY AREA

Mangrove forests in the mainland portion of Biscayne National Park, at the southern tip of the Florida peninsula, were selected for study

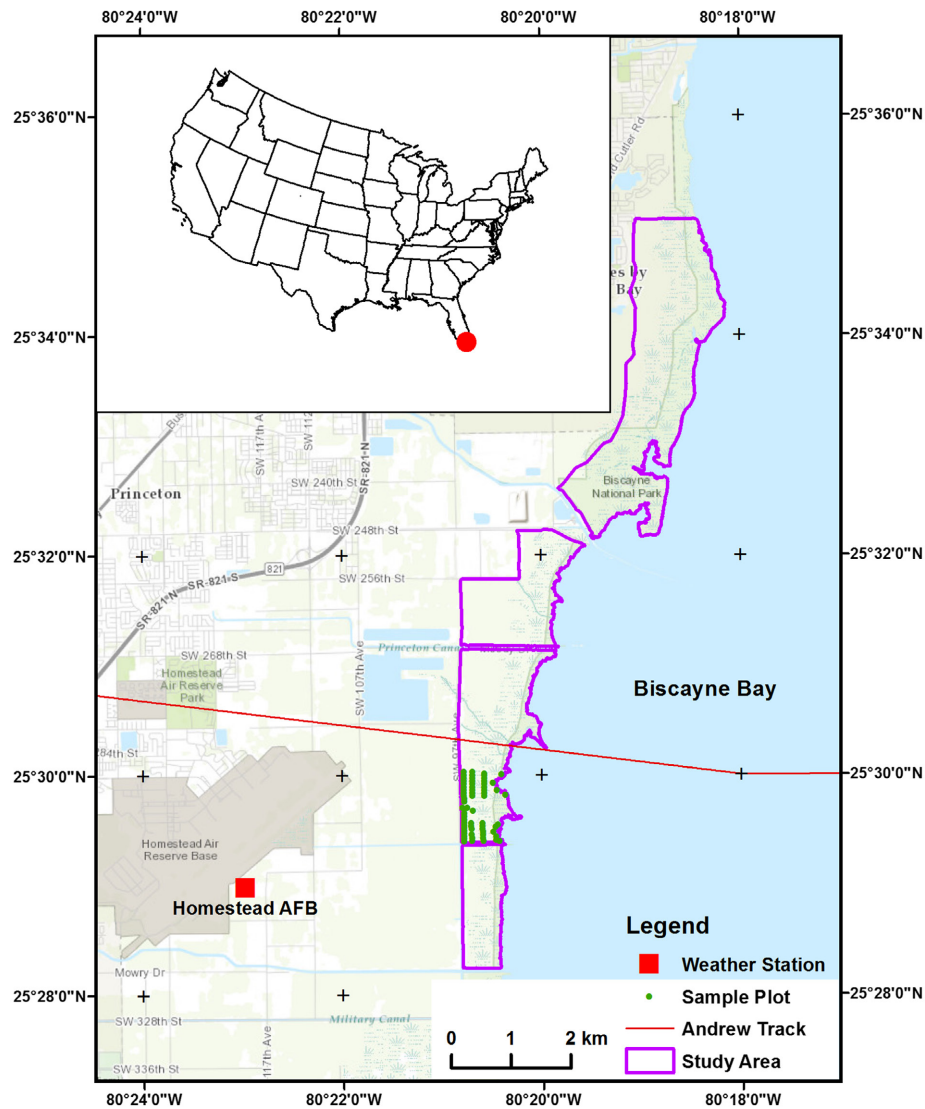


Fig. 1. The study area in South Florida.

(Fig. 1). Located at approximately 25°32' N latitude and 80°20' W longitude, the study area comprises a continuous strip of mangrove forest of approximately 14 km length. It is bounded on the south by the Mowry Canal (C-103), on the east by Biscayne Bay, on the west by the L-31E canal, and extends north to the Park boundary. The area is divided into compartments by drainage ditches and canals that run from east to west. Soil varies from relatively deep peats close to Biscayne Bay to calcareous muds in the interior (Ross et al. 2001). The elevation of the study area is between -0.3 to

+0.5 m (NAVD 88) and the tidal range is about 0.6 m according to the tide gauge at Virginia Key (www.noaa.com), about 30-km distant. The area's subtropical climate is characterized by average temperatures of 28–29°C in June, July, and August, and 20–21°C in December, January, and February, with chilling events occurring during the cold winters. The mean annual precipitation of 1300 mm is concentrated from May to October, with two peaks in June and September. Hurricanes that impact the area may approach from either the Atlantic Ocean or Gulf of Mexico. Hurricanes that made landfall

near the study area during the study period (1985–2011) include Andrew (1992), Katrina (2005), and Wilma (2005). Katrina as a tropical storm and Wilma as a Category one hurricane generated maximum 1-min sustained surface wind speeds of 28–30 m/s and 36–39 m/s, respectively, without causing significant storm surges in the study area (www.aoml.noaa.gov/hrd). Andrew made landfall as a Category 5 hurricane in the study area on 24 August, 1992, with a maximum 1-min sustained surface wind speed of 55–60 m/s (Powell and Houston 1996), resulting in a storm surge of 2.5–4.5 m above NAVD 88 (Zhang et al. 2013).

The predominant vegetation of the study area consists of four woody plant species: *Rhizophora mangle* (red mangrove), *Avicennia germinans* (black mangrove), *Laguncularia racemosa* (white mangrove), and *Conocarpus erectus* (buttonwood). Mangrove composition and structure vary consistently from coast to interior. Tall red mangrove is dominant close to the coast, though stands dominated by black or white mangrove are also found. Canopy height decreases inland, with a mixed species assemblage prevailing through communities with canopy heights down to 1 m, and then red mangroves again becoming dominant further inland (Ross et al. 2001). The mangroves along this gradient are categorized as fringe, transition, and dwarf forests (Ross et al. 2009), respectively, according to the classification system of Lugo and Snedaker (1974). Buttonwoods occur along the canals and drainage ditches, and are found mixed with other mangrove species in small, isolated tree islands in the dwarf forest.

DATA

Meteorological records

Meteorological data, including temperature, precipitation, and wind speed, came from the Homestead Air Force Base (AFB) station with a World Meteorological Organization (WMO) number of 722,026, about 4 km from the study site (Fig. 1). The zipped integrated surface hourly data were downloaded from the National Climatic Data Center of National Oceanic and Atmospheric Administration (<http://www1.ncdc.noaa.gov/pub/data/noaa/>). The data were processed in the statistical software R (<http://www.r-project.org/>) to extract hourly temperature, precipitation, and

wind speed for calculation of statistics during a given time period (e.g., a month).

Landsat images

The surface reflectance images for the scene (path 15 and row 42) were acquired from the U.S. Geological Survey (USGS) through Earth Explorer (<http://earthexplorer.usgs.gov/>). The images were generated using specialized software called Landsat Ecosystem Disturbance Adaptive Processing System (LEDAPS) (USGS 2015). LEDAPS uses the 6S radiative transfer approach to reduce noise from atmospheric scattering and absorption in Landsat TM images (Vermote et al. 1997, Masek et al. 2006). The error of atmospheric correction in LEDAPS data is reported to be about 5% of the measured reflectance (Masek et al. 2006). LEDAPS surface reflectance images have been used in analysis of forest disturbance in several recent studies (Masek et al. 2008, Townsend et al. 2012, Zhu et al. 2012, Thapa 2014). Cloud-free Landsat 4–7 images of the study area from 1985 to 2011 were downloaded and used to calculate the vegetation indices and conduct change detection. Three Landsat 4, 125 Landsat 5, and 22 Landsat 7 TM images were analyzed. More images were available from December to April due to clear skies during that period, and fewer from May to November due to high cloud coverage.

LiDAR data

The LiDAR data used in this study were collected in 2007 by 3001 Inc., under contract with the Florida Division of Emergency Management. The spacing of LiDAR measurements averaged 1.3 m, producing an average density of two points per square meter. An accuracy assessment was performed by calculating elevation differences between ground control points and filtered LiDAR points, which represent bare-earth elevations (3001 Inc. 2008). The vertical root-mean-square (RMS) errors of the LiDAR data are less than 0.15 m in urban areas.

METHODS

Calculation of vegetation indices

Dimensionless vegetation indices use a combination of radiometric measures from satellite images to indicate the relative abundance and

activity of green vegetation (Jensen 2015). Numerous vegetation indices have been developed since the 1960s, some of them requiring high-resolution spectral reflectance data for calculation. Landsat satellites use a coarse resolution of spectral bands covering visible, near infrared (NIR), and shortwave infrared (SWIR) spectra, and thus can only be used to calculate a limited subset of vegetation indices. The sensitivity in change detection of four frequently used indices, i.e., NDVI, NDMI, SAVI, and EVI, were compared in this study. NDVI is defined as:

$$\text{NDVI} = \frac{\rho_4 - \rho_3}{\rho_4 + \rho_3} \quad (1)$$

where ρ_3 and ρ_4 are the reflectance values from band3 (red) and band4 (NIR) of a Landsat image, respectively. NDVI has been used extensively to estimate vegetation properties (Jensen 2015), despite being prone to noise from variation in atmospheric and soil conditions, and tending to saturate with increasing vegetation density (Huete 1988, Gao 1996). SAVI and EVI were proposed to reduce the background noise and the saturation at the high end of vegetation density (Huete 1988, Huete et al. 2002). SAVI and EVI are defined as:

$$\text{SAVI} = \frac{\rho_4 - \rho_3}{\rho_4 + \rho_3 + L} (1 + L) \quad (2)$$

$$\text{EVI} = G \frac{\rho_4 - \rho_3}{\rho_4 + C_1 \rho_3 - C_2 \rho_1 + S} \quad (3)$$

where ρ_1 represents the reflectance values of band1 (blue). L , a canopy density adjustment factor that relies upon the proportional cover of the vegetation vs. bare soil, was set to be 0.5 in this study (Huete 1988). C_1 and C_2 use the blue band to correct the red band for atmospheric aerosol scattering, S adjusts the soil factor, and G is a gain factor. The values of G , C_1 , C_2 , and S were empirically set to be 2.5, 6.0, 7.5, and 1.0, respectively, following Huete et al. (1994, 1997).

NDMI, which is defined as

$$\text{NDMI} = \frac{\rho_4 - \rho_5}{\rho_4 + \rho_5} \quad (4)$$

was proposed by Hardisky et al. (1984) and Gao (1996) to assess the biomass and moisture content in vegetation, where ρ_5 represents the reflectance values of band5 (SWIR). In several studies, NDMI performed better than NDVI in documenting the effects of harvesting and hurricane disturbance on forests (Wilson and Sader 2002, Wang et al. 2010), and thus was included in this study. NDMI values vary from -1 to $+1$, with high values associated with large biomass and water content. NDVI values likewise range from -1 to 1 , but are between 0 and 1 for vegetation because ρ_4 is typically larger than ρ_3 . The values of SAVI and EVI are not mathematically guaranteed to be between -1 and 1 , but they are usually close to this range. Therefore, NDVI, NDMI, SAVI, and EVI derived from the Landsat TM reflectance images were compared directly for detecting mangrove changes.

A python script was developed in ArcGIS to automatically calculate the vegetation indices for 150 images. First, the downloaded images were unzipped; second, the images enclosed by the polygon of the study area were extracted using the ArcGIS Clip tool; finally, the vegetation indices for each pixel in the study area were calculated using Eqs. 1–4.

Classification of mangroves using canopy heights from LiDAR

Previous research indicated that in some areas, tall fringe mangrove forests close to the coast and interior dwarf mangrove forests differ in their responses to hurricane and chilling events (Ross et al. 2006, 2009). Therefore, airborne LiDAR data collected by the Florida Division of Emergency Management in 2007 was employed to map tree heights and distinguish areas of tall and dwarf mangroves. The $1500 \text{ m} \times 1500 \text{ m}$ LiDAR data tiles covering the study area in binary las format (<http://www.asprs.org/Committee-General/LASer-LAS-File-Format-Exchange-Activities.html>) were downloaded from the data distribution site (<http://fldem.ihr.c.fiu.edu/fldem-lidar20120119/Default.aspx>). A three-step procedure was then employed to estimate tree heights. The initial step was to derive a digital terrain model (DTM) from the downloaded las LiDAR data set. As ground and nonground points were already identified in the las data set, a terrain data set was first created using multiple tiles

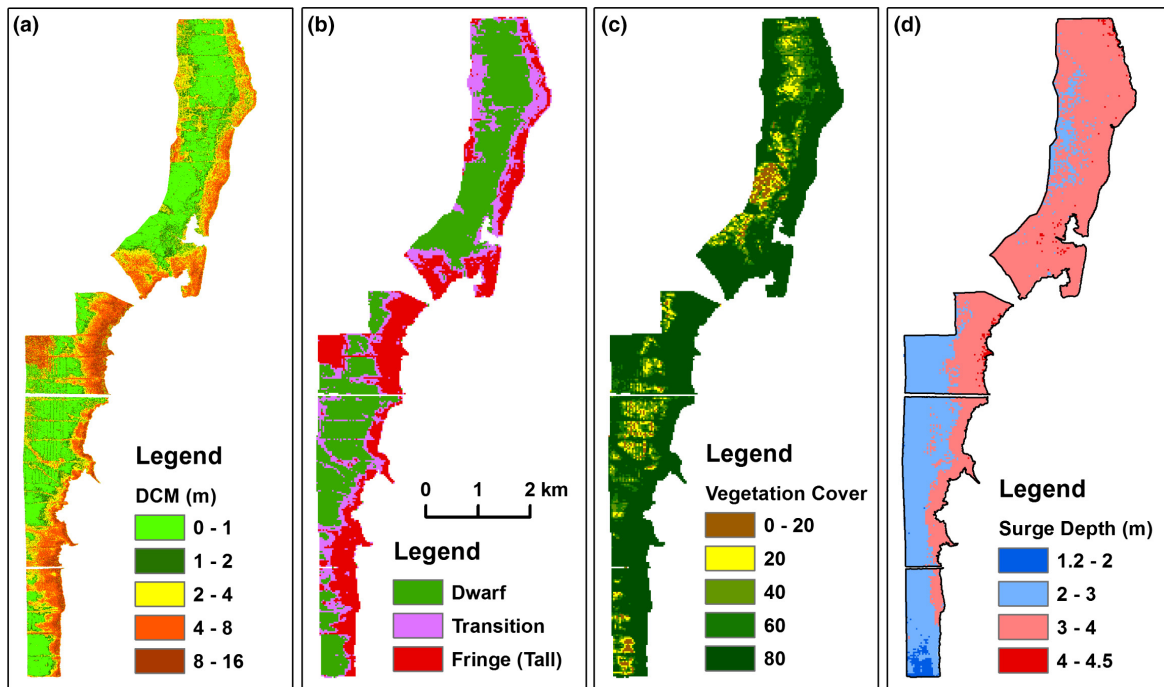


Fig. 2. The LiDAR digital canopy model with a cell size of 1 m (a), the classified mangrove zones with a cell size of 30 m (b), the percentage of vegetation coverage with a cell size of 30 m (c), and the inundation depth of storm surges caused by Hurricane Andrew (d), which was derived by subtracting LiDAR DTM from the computed maximum storm surge.

of las ground points and the boundary polygon of the study area as a soft clip based on a triangulated irregular network in ArcGIS. Then, a $1\text{ m} \times 1\text{ m}$ DTM of the study area was created by applying the Terrain to Raster tool to the terrain data set. The second step was to derive a digital surface model (DSM). First, a mosaic data set with a cell size of 1 m was created using all points in the las LiDAR data set in ArcGIS, and then a $1\text{ m} \times 1\text{ m}$ DSM was created by clipping the mosaic data set using the polygon of the study area. The third step was to derive a digital canopy model (DCM) by subtracting the DTM from the DSM. The values of the DCM in areas with few trees could be negative due to the difference between the methods used to generate the DTM and DSM (Zhang et al. 2008); if so, these were replaced with a zero value using the raster algebra tool in ArcGIS.

As the dwarf mangrove forest consists mainly of trees $<2\text{ m}$ high, and the fringe mangrove forest comprises trees $4\text{--}18\text{ m}$ high (Ruiz et al. 2008), the

study area was classified into three zones, including dwarf (with DCM values $<2\text{ m}$), transition (DCM values of $2\text{--}4\text{ m}$), and fringe (DCM values $>4\text{ m}$) mangroves based on canopy heights. In order to generate a $30\text{ m} \times 30\text{ m}$ canopy classification image that matched with vegetation index images from Landsat, a $30\text{ m} \times 30\text{ m}$ DCM was first generated by averaging $1\text{ m} \times 1\text{ m}$ DCM values, and then classified into tree height categories (Figs. 2a and b), yielding areal estimates of 6.7 , 3.0 , and 3.8 km^2 for the dwarf, transition, and fringe mangroves, respectively. A map of the percentage of vegetation coverage was also generated through counts of pixels of the $1\text{ m} \times 1\text{ m}$ LiDAR DCM with heights greater than 0.3 m within a $30\text{ m} \times 30\text{ m}$ cell (Fig. 2c). LiDAR DCM pixels with height values less than 0.3 m (two times the typical LiDAR vertical RMS error) were defined as terrain pixels without vegetation.

The canopy height map was examined through a comparison with tree heights measured at 67 sample plots (Fig. 1) in 2002, following the procedure described in Ruiz et al. (2002). The maximum

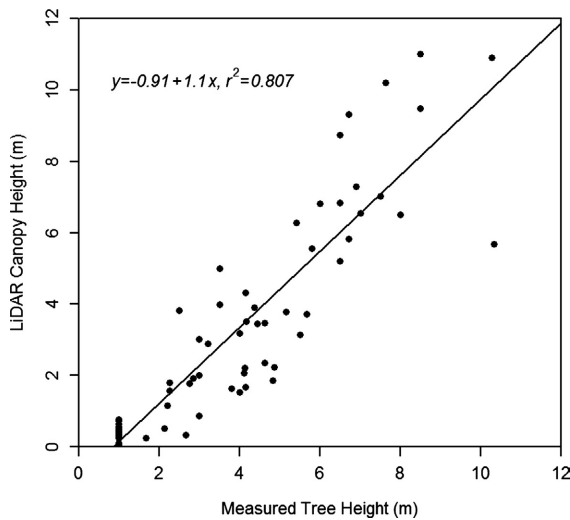


Fig. 3. The relationship between the tree heights measured in the field and LiDAR canopy heights.

height of each tree species was measured at 0, 5, and 10 m along the centerline of a 10 m × 1 m plot oriented N–S. Species maxima per plot were averaged to calculate canopy height. The 1 m × 1 m LiDAR DCM was resampled into a 10 m × 10 m image using the bilinear interpolation method in ArcGIS to compare the LiDAR measurements with measured tree heights in the field. The results showed that the LiDAR DCM and the field tree heights had a good agreement with some discrepancy (Fig. 3), which was expected because the LiDAR and field data were not collected simultaneously and the two methods differed in how canopy height was calculated. Thus, the LiDAR DCM represented the overall canopy pattern in the study area well, though it was only a snapshot of vegetation at a particular moment.

Evaluation of the performance of vegetation indices

The most commonly used method to determine the effectiveness of vegetation indices from Landsat images in depicting changes caused by disturbances is to compare the vegetation index change maps with a reference consisting of ground observed data, aerial photographs, or high-resolution satellite images (Jensen 2015). The relative performance of the indices is then assessed through the statistical analysis of the error matrix between the change maps and reference data. However, the method is limited by the availability

of historical reference data in the study area. An alternative method that compares the distributions of disturbance-initiated vegetation index changes with the distributions of the background variation in the absence of disturbance was employed in this study. First, vegetation index differences (ΔVI s) were generated using the equation:

$$\Delta VI_i = VI_i - VI_j \quad (5)$$

where VI_i and VI_j represent the vegetation indices at time i and j ($i > j$), respectively.

Then, image pairs free from the influence of freeze and hurricane events, collected in the same month and contiguous years in order to minimize seasonal effects, were selected to estimate the background variation of vegetation indices. A total of 12 pairs of images met the selection conditions, and index differences from all pairs were combined to derive a distribution of background variation. Finally, the significance of differences between potential event and background distributions were examined using nonparametric Kolmogorov–Smirnov test (Davis 2002). Cohen’s d index (Ellis 2010) was employed to estimate the separation between the event and background distributions to measure the effectiveness of the index in change detection.

$$d = \frac{m_e - m_b}{s} \quad (6)$$

where m_e and m_b are the means of the vegetation index differences for the event and background variation. The parameter s is related to the standard deviations of the vegetation index differences by

$$s = \sqrt{\frac{(n_e - 1)s_e^2 + (n_b - 1)s_b^2}{n_e + n_b - 2}} \quad (7)$$

where n_e and n_b are the total number of pixels of the vegetation index difference images for the event and background variation, respectively, and s_e and s_b are the standard deviations of the respective index difference images. The larger the absolute value of Cohen’s d , the more sensitive the vegetation index is to change. As the distributions of various different vegetation indices for the background variation are similar (Fig. 4), d is mainly determined by the mean and standard deviation of

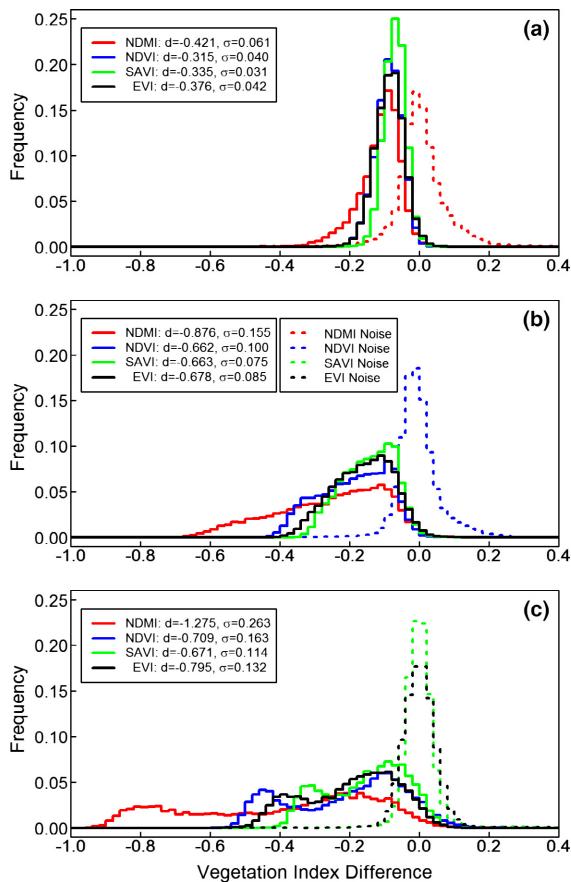


Fig. 4. The distributions of vegetation index difference values for pairs of images: (January 8, 1987, April 30, 1987) (a), (November 10, 1988, April 6, 1990) (b), and (November 19, 1991, March 29, 1993) (c). The parameters d and σ represent Cohen's d and the standard deviation of the difference values, respectively, in the study area. The first case represents a typical seasonal change; the second case an intense chilling event, the third case an intense hurricane. The solid lines represent the distributions of the vegetation indices for the seasonal change and events, while the dashed lines represent the distributions of the vegetation indices for the background variations (noises).

a vegetation index for the event. A larger absolute value of the event mean indicates a better separation between the event and background variation by a vegetation index. The interpretation of the event standard deviation in change detection is more complicated. On one hand, a smaller event standard deviation increases the likelihood of detecting event-induced change in the study area.

On the other hand, the larger the event standard deviation (the broader the distribution), the higher the capacity of an index to express levels of vegetation change within an area (Wang et al. 2010).

Quantification of mangrove dynamics

Both spatial and temporal aspects of mangrove forest change were analyzed. To quantify the magnitude of change in space, pixels with large ΔVIs were identified using a threshold (VT_i) based on the mean values ($\mu_{\Delta VI,i}$) of the difference image and a fixed standard deviation ($\sigma_{\Delta VI}$):

$$\begin{aligned}
 VT_i &= \mu_{\Delta VI,i} + m\sigma_{\Delta VI} \text{ for identifying pixels} \\
 &\text{with large increase in } \Delta VI \\
 &\mu_{\Delta VI,i} - m\sigma_{\Delta VI} \text{ for identifying pixels} \\
 &\text{with large decrease in } \Delta VI
 \end{aligned} \quad (8)$$

where m is an empirical value which was set to be two. As the mean values of the vegetation index difference images for various time periods were not constant, inclusion of the mean index value of a given difference image into Eq. 8 served to standardize the baseline for identifying large change pixels. For comparative purposes, large change pixels in each difference image were identified by a common threshold distance ($m\sigma_{\Delta VI}$) from $\mu_{\Delta VI,i}$. The parameter $\sigma_{\Delta VI}$ was estimated by averaging the yearly standard deviations of the vegetation index difference images from April and December, the two months between which the vegetation index difference was usually largest. If images for April or December were not available, the images in adjacent months were used as surrogates. The average standard deviation $\sigma_{\Delta VI}$ mainly represented the variation from seasonal changes and background random noise. For an index difference image impacted by chilling events or hurricanes, pixels with a decrease in index value (typically negative) less than the threshold determined by Eq. 8 were characterized as severely damaged in a relative sense, while pixels with a decrease larger than the threshold were considered mildly damaged.

The mean vegetation indices for the entire study area, the combined dwarf and transition mangrove zones, and the fringe mangrove zone were calculated and analyzed for seasonal and episodic changes from hurricanes and chilling events. The analysis required that the seasonal change signal

be separated from variation induced by episodic events. A harmonic analysis was employed to estimate the magnitude and phase of seasonal change after the long-term linear trend was removed (Pugh 1996, Zhang et al. 2000, Zhu et al. 2012), as:

$$VI_i = VI_0 + H \cos(2\pi t_i / \omega + \phi) \quad (9)$$

where VI_i is the vegetation index at time i and VI_0 represents the mean vegetation index during the analysis period; H is the amplitude, t_i is time in years, ω is the frequency, expressed as yr^{-1} , and ϕ is the phase of the seasonal change. The values of VI_0 , H , and ϕ were estimated in R using a least squares fit based on vegetation indices from 150 Landsat TM images.

The magnitude of disturbances from hurricanes and chilling events as well as the recovery rates from them were analyzed after seasonal variation was removed from the time series of vegetation indices. In order to separate the changes caused by disturbances from background variation, the NDMI residuals between 1989 and 1998, 2005 and 2006, 2010 and 2012, during which disturbances had obvious effects on the residuals, were removed from the time series. Then the standard deviation of the remaining residuals which represented the background variability was calculated. Finally, the negative values of two or three

standard deviations were used to separate the disturbance signals from the background variation.

Identifying chilling events from temperature records

As early as 1766, winter temperatures that reach the freezing point have been reported in South Florida, in accordance with its subtropical climate (Olmsted et al. 1993). Typically, freezing temperatures last for no longer than 6–8 h. The low temperature often causes severe defoliation and can even kill mangrove trees, resulting in a sudden collapse in mangrove forest density in particular years. In the study area, Ross et al. (2009) observed damage in the dwarf mangrove forest in two occasions when temperatures at the Homestead AFB station were about 3°C or less (January 1996 and 2001), but not when minimum temperatures were higher. During the 1996 and 2001 events, the temperatures inside the dwarf mangrove forest were 2–3°C lower than at Homestead AFB. Hence, a chilling event was defined as an instance during which the temperature at the Homestead AFB station was 3°C or less in a single or consecutive days. A chilling event in this paper represents the meteorological conditions that produce symptoms usually associated with freeze damage in plants, regardless of whether or not true freezing temperature was reached. The minimum

Table 1. Observed chilling events in Biscayne Bay, Florida based on the meteorological records at the Homestead AFB station.

Chilling event	Date	Lowest temperature (°C)	Duration (h)	Intensity (°C h)	No. events
1985	01/22/1985	-0.5	10	22.9	1
1989	02/25/1989	2.2	2	1	2
	12/24/1989	0.6	9	30.2	
1996	12/25/1989	0.6	11		3
	01/09/1996	2.2	1	0.8	
	02/05/1996	2.2	6	3.8	
	02/17/1996	2.2	2	1.1	
2001	01/05/2001	3	6	0	1
2003	01/24/2003	3	3	0	1
2008	01/03/2008	1.8	5	3.7	1
2009	02/05/2009	2.7	1	0.3	1
2010	01/06/2010	3	1	0	4
	01/10/2010	1.3	8	29.3	
	01/11/2010	-0.6	9		
	12/14/2010	1.8	3	7.4	
	12/15/2010	1.5	7		
	12/28/2010	4	1.2	3.2	

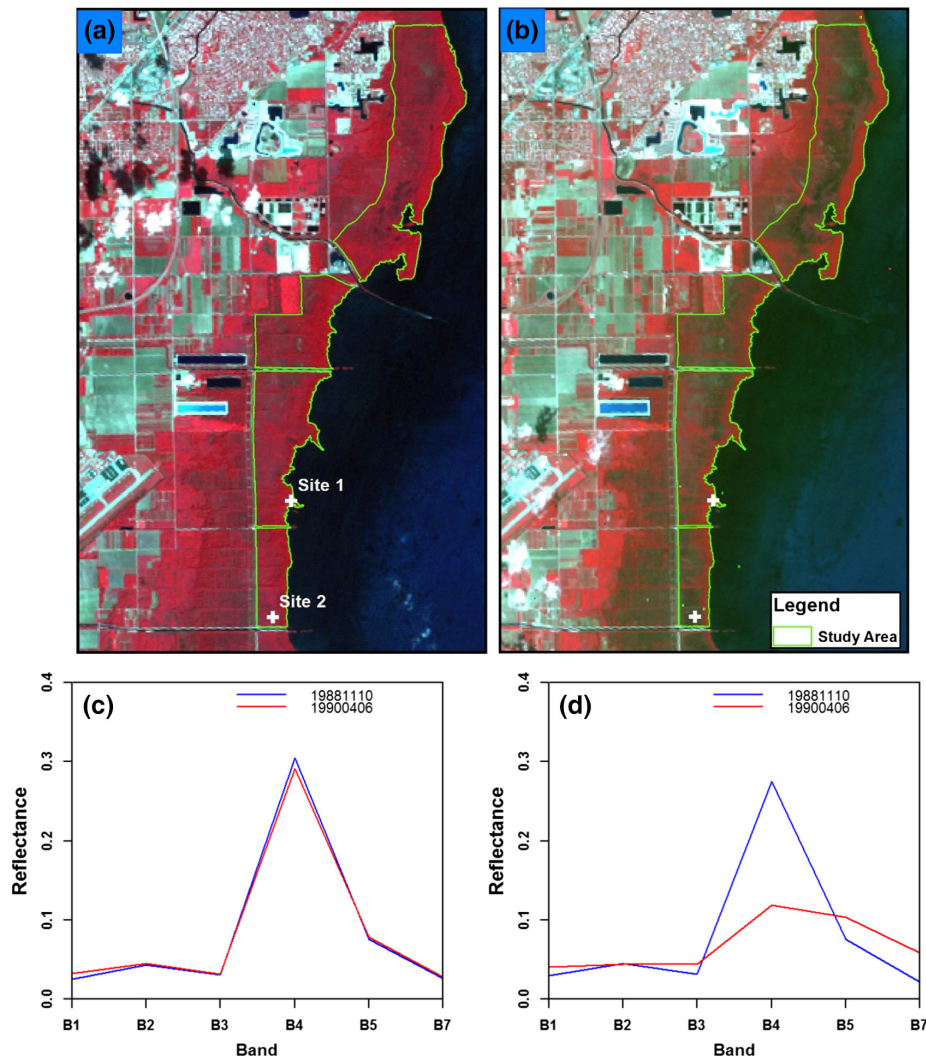


Fig. 5. The false color composites of Landsat 5 TM NIR (band 4), red (band 3), and green (band 2) surface reflectance on November 10, 1988 (a) and April 6, 1990 (b). The reflectance of bands 1–5 and band 7 of Landsat images at two selected locations representing small (c, Site 1) and large impacts (d, Site 2) experienced by the chilling events of 1989.

temperatures, durations, and intensities of all chilling events over the period 1985–2011 were calculated in R on the basis of the Homestead AFB meteorological record (Table 1). The intensity of a chilling event was defined as the total area above the hourly temperature curves and below the 3°C threshold line. Chilling intensity (CI) was expressed in units of °C/hr calculated as:

$$CI = \sum_{i=1}^N (3 - T_i) \Delta t \quad (10)$$

where Δt is equal to 1 h, T_i are hourly temperatures less than or equal to 3°C during a chilling event, and N is the total number of such hourly temperatures during the period.

RESULTS

Vegetation indices

Vegetation changes between sequential Landsat images were represented by the variation in the spectral reflectance of six bands, which responded to the same driving forces that affected the

mangrove forest (Fig. 5). As NDVI, SAVI, EVI, and NDMI used different combination of spectral bands, it was expected that one index would perform better than the others in detecting mangrove changes. The question was whether one of the indices was consistently superior. The difference images from three TM 5 image pairs which represented a typical seasonal change without disturbance in 1987, a severe chilling event in 1989, and a major hurricane in 1992 were analyzed in order to compare the performance of four vegetation indices (Fig. 4). When applied to seasonal change and the change associated with chilling or hurricane, the difference distributions of all four indices differed significantly from background variations, with a P value of 0.001 based on the Kolmogorov–Smirnov test. The distribution of the SAVI difference values from a seasonal change (Fig. 4a), which was narrowest and almost symmetric around the mean value, had the second smallest absolute d value and the smallest standard deviation. The absolute d values and standard deviations of NDVI and EVI were also relatively small, and the distributions were slightly broader than those of SAVI. NDMI had an asymmetric distribution with a tail toward the negative side, and had the largest absolute d value and standard deviation. Therefore, NDMI was the best index for detecting seasonal change in the mangroves of the study area. In the case of the 1989 chilling event (Fig. 4b), the distributions, d values, and standard deviations of NDVI, SAVI, and EVI were similar. NDMI had the largest absolute d value and exhibited the widest spread of difference values, indicating that it was best in distinguishing disturbance from a chilling event. In the case of Hurricane Andrew in 1992 (Fig. 4c), NDMI, was again the most capable of the four indices to detect damage to the mangrove forest, based on a much larger absolute d value and standard deviation. The presence of two peaks in the distributions of difference values for all four indices is noteworthy, and implies two distinctive levels of disturbances in the study area in response to the hurricane's impact. In summary, NDMI performed best in indicating not only seasonal change but also changes induced by chilling events and hurricanes. Additionally, the Kolmogorov–Smirnov tests showed that the NDMI distributions differed significantly from the NDVI, SAVI, and EVI

distributions; therefore, NDMI was used for analysis of spatial and temporal change in mangroves in the remainder of this paper.

Spatial variation of mangrove changes

Normalized difference moisture index values from the same image pairs used to compare vegetation indices were employed to illustrate the spatial variation in mangrove forests. In years without major disturbance, the NDMI value of the mangrove forest nevertheless exhibited seasonal variation, i.e., NDMI was high in December or January depending upon the initial time of cold temperature onset, and lower in March or April, as illustrated for 1987 in Fig. 6a and b. It is noteworthy that NDMI values were larger in the fringe forest than the dwarf mangrove in both December and March 1987. The values of the difference image between December and March were small, most between -0.2 and 0.0 (Fig. 6c). In this typical year, only small areas of mangroves scattered over the interior of the study area had difference values lower than the threshold VT_i estimated by Eq. 8, probably indicating a severe local defoliation of unknown cause (Fig. 6d).

Normalized difference moisture index values in dwarf and fringe mangroves mostly ranged from 0.4 to 0.6 and 0.6 to 0.8 , respectively, before the chilling event of 1989 (Fig. 7a). The NDMI values of both dwarf and fringe mangroves decreased following the disturbance. The decrease in NDMI was larger in the dwarf forest than in the fringe forest, with negative values of NDMI occurring in patches in the dwarf mangroves (Fig. 7b). In most portions of the fringe forest, the difference values of NDMI were negative, in the range of -0.2 to 0 , while the difference values in most of the dwarf forest ranged from -0.6 to -0.2 , with values of -0.95 to -0.6 in some areas (Fig. 7c). Severely impacted areas which were below the threshold VT_i occurred in the dwarf mangroves, and accounted for an area of 2.3 km^2 (17%) of the 13.5 km^2 study area (Fig. 7d). One year after the chilling event, NDMI values of the fringe mangroves recovered to above 0.6 . While NDMI values in some dwarf mangrove areas recovered to the range of 0.4 – 0.6 , NDMI reached only to 0.2 – 0.4 in most of the dwarf forest (Fig. 7e). The difference values of NDMI in most dwarf and fringe mangroves were positive, except for a small area

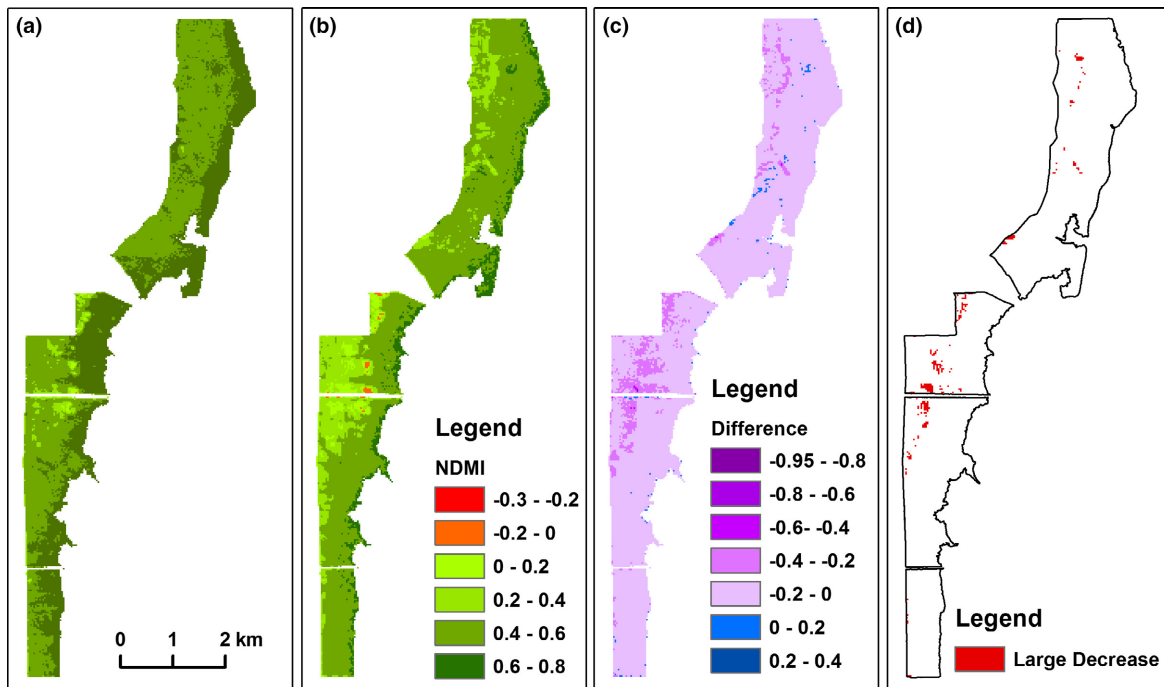


Fig. 6. The NDMI index on January 8, 1987 (a), on April 3, 1987 (b), the NDMI difference image (c), and the areas where the NDMI difference is less than the threshold calculated by Eq. 8 (d).

in the northern part of the dwarf forest (Fig. 7f). This indicated that both dwarf and fringe forests experienced recovery after the 1989 chilling event, and the largest increase in NDMI occurred in the middle of the dwarf mangroves (Fig. 7g). Two years after the chilling event, NDMI values in most dwarf and fringe mangrove areas had recovered to pre-event levels, while NDMI in a few locations in the dwarf forest remained lower than before the chilling event (Fig. 7h).

Before Hurricane Andrew, in November 1991, NDMI values within a range of 0.4–0.6 predominated in the dwarf forest and values between 0.2 and 0.4 were secondary (Fig. 8a). In contrast, values of 0.6–0.8 were most common in the fringe forest and values of 0.4–0.6 were less frequent. After Andrew, NDMI values were reduced to a range of 0–0.2 in the dwarf forest and a range of –0.3–0 in the fringe forest (Fig. 8b). The NDMI difference image showed that NDMI values were lower in 98% (13.2 km²) of the study area, and only a small area exhibited an increase in NDMI (Fig. 8c). The largest decrease in NDMI occurred in the fringe forest (Fig. 8d), indicating that it experienced the major impact from Andrew. One

year after Andrew, NDMI values in the dwarf mangrove forest recovered to the range of 0.4–0.6, whereas NDMI values in some fringe mangroves recovered to the positive range of 0–0.2, while NDMI values in the remaining fringe mangroves were still negative (Fig. 8e). The NDMI difference image between April 1993 and December 1993 showed that recovery was evident throughout the area but variable in magnitude (Fig. 8f) and only a small portion in the dwarf mangrove zone had experienced faster recovery (Fig. 8g). Two years after Andrew, NDMI values in the dwarf forest had recovered and even exceeded the pre-hurricane values; however, the fringe mangroves were still in the middle trajectory of recovery, and had not reached prehurricane values (Fig. 8h).

As illustrated in Figs. 7 and 8, the dwarf and fringe mangrove zones responded differently to disturbances from chilling events and hurricanes, and this difference appeared to be related to canopy height. In order to verify the relationship, disturbances from chilling events or hurricanes were classified into mild and severe categories, based on whether NDMI difference values were less than a threshold given by Eq. 8. Fig. 9 shows that the

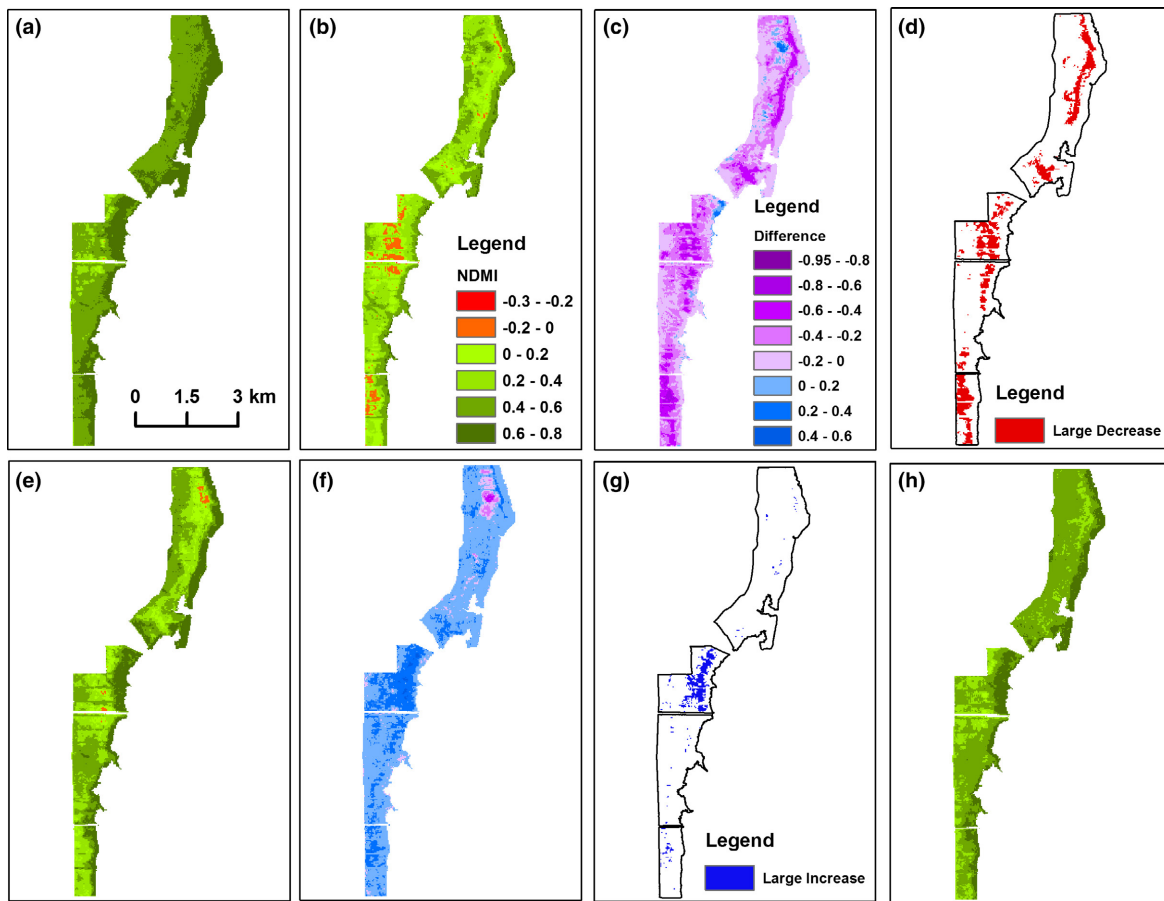


Fig. 7. The NDMI index on November 10, 1988 before the chilling event (a), the NDMI index on April 6, 1990 after the chilling event (b), the NDMI difference image between the indices on November 10, 1988 and April 6, 1990 (c), the areas where the NDMI difference was less than a given threshold (d), the NDMI index on December 18, 1990 (e), the NDMI difference image between the indices on April 6, 1990 and December 18, 1990 (f), the areas where the NDMI difference was larger than a given threshold (g), and the NDMI index on November 19, 1991 (h).

percentage of mildly disturbed area due to chilling events, represented by small negative NDMI differences, decreased slightly as canopy height increased from 0.25 to 0.75 m and then increased slowly after 0.75 m, reaching maximum at a height of 9.75 m. The percentage of severely disturbed area, represented by large negative NDMI difference values below the threshold VT_i , was greatest at 0.75 m, the same height that mild chilling was lowest, then decreased gradually before becoming negligible beyond 7 m height. The average percentages of severely disturbed forest were 22%, 18%, and 5%, respectively, in dwarf, transition, and fringe mangroves. In contrast to the changes caused by the chilling event, the percentage of

area with severe disturbance from Hurricane Andrew was negligible in the dwarf forest, increased drastically in the transition forest and peaked in the fringe forest (Fig. 9). The average percentages of severely disturbed area were 2%, 33%, and 84%, respectively, in dwarf, transition, and fringe mangroves. The percentage of mild hurricane disturbance was largest in the dwarf forest, dropping off quickly in the transition forest and becoming insignificant in the fringe forest.

Temporal variation of mangrove changes

As chilling disturbances were concentrated in the dwarf and transition mangrove zones and hurricane disturbances were focused

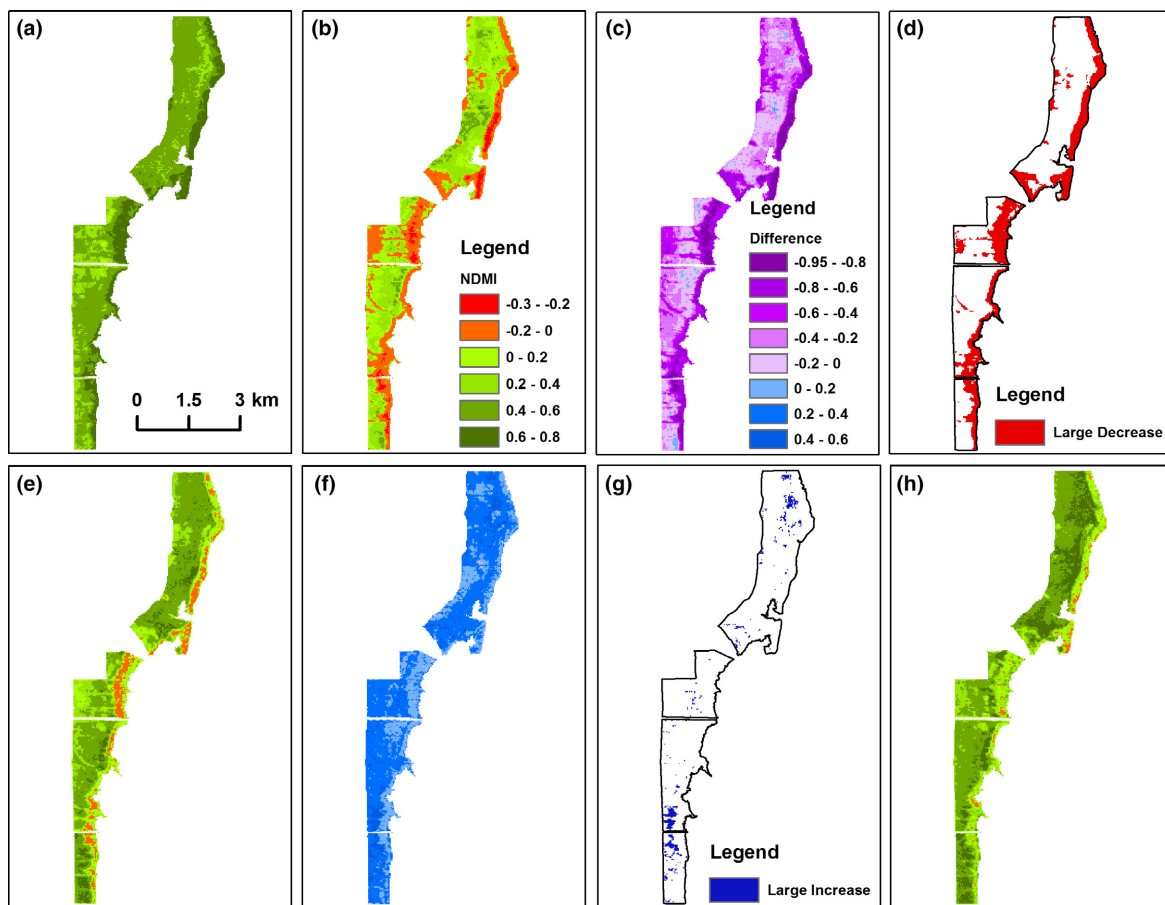


Fig. 8. The NDMI index on November 19, 1991 before Hurricane Andrew (a), the NDMI index on March 29, 1993 after Andrew (b), the NDMI difference image between the indices on November 19, 1991 and March 29, 1993 (c), the areas where the NDMI difference was less than a given threshold (d), the NDMI index on December 10, 1993 (e), the NDMI difference image between the indices on March 29, 1993 and December 10, 1993 (f), the areas where the NDMI difference was larger than a given threshold (g), and the NDMI index on November 27, 1994 (h).

primarily in the fringe zone, two time series of mean NDMI were generated for the fringe zone and a combined dwarf–transition zone to analyze temporal changes in the mangrove forest. A time series of mean NDMI values based on the entire study area was also generated for comparison. The mean NDMI values for the study area did not show any significant linear trend, with an R^2 value of 0.017 and P value of 0.11 (Davis 2002), though the sequence included seasonal fluctuations and large deviations caused by hurricanes and chilling events (Fig. 10). The peak NDMI values occurred in December in a season lacking severe chilling

or hurricane disturbances, slightly before the month (January) with lowest average temperature. The period of high precipitation, May to October, aligned approximately with the period of rising NDMI, although NDMI continued to increase through December.

The NDMI of the dwarf–transition zone likewise did not show a significant linear trend, with an R^2 value of 0.007 and P value of 0.30 (Fig. 11a). The magnitude of seasonal change was about 0.11 with a phase of 47 d, indicating that the NDMI reached a trough in May and a peak in November. The effect of the phase value was equivalent to shifting the cosine curve toward the left by

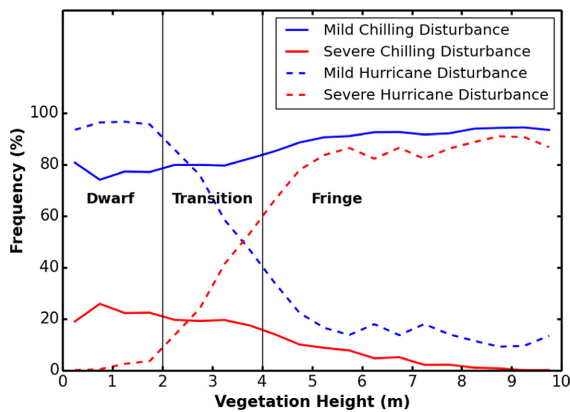


Fig. 9. The percentage of the mild damage area caused by the chilling event in 1989 at various canopy heights, the percentage of severe damage caused by the chilling event in 1989, the percentage of mild damage caused by Hurricane Andrew, and the percentage of severe damage caused by Andrew.

47 d along the “Time” axis in Fig. 11 if January 1 is assumed to be day zero. The least squared fit for the seasonal change was statistically significant, generating R^2 and P values of 0.28 and 0.0, respectively. The residuals of the NDMI after the seasonal components were removed still exhibited considerable fluctuation. The largest decrease in NDMI residuals was caused by the chilling event in December 1989. It is noteworthy that NDMI did not reach its lowest point immediately after the chilling event, instead reaching a minimum in April 1990. The mean NDMI value of the dwarf and transition mangroves almost

recovered to the pre-event level 2 yr later. As a category 5 hurricane in 1992, Andrew stopped the recovery process, but did not result in the large decrease of NDMI values in the dwarf and transition mangroves, as hurricane disturbance was mild there. The NDMI value in the dwarf–transition forest in December 1993 was approximately at the same level as in December 1988, showing that the dwarf–transition mangroves recovered quickly from the double impact of the chilling event in 1989 and the hurricane in 1992. Katrina as tropical storm and Wilma as category one hurricane that made landfall near the study site in 2005 did not cause visible changes in mean NDMI in the dwarf and transition forests. In addition to the chilling events in 1989, mean NDMI was reduced in response to a chilling event in December 2010. The response of the dwarf–transition forest to the chilling event in January 2010 was not evident in NDMI, though chilling intensity was comparable to that of the 1989 event. Other chilling events with intensities smaller than that of the 1989 event did not cause large decreases in NDMI, indicating that these events did not result in severe or extensive damage in the dwarf and transition forests.

The NDMI of the fringe mangroves show a very weak linear trend of increase, with an R^2 value of 0.026 and a P value of 0.05 (Fig. 11b). The magnitude of seasonal change was about 0.1 and the phase was 22 d, indicating that NDMI reached a trough in June and a peak in December. The least squared fit for seasonal change was statistically significant, generating R^2 and P

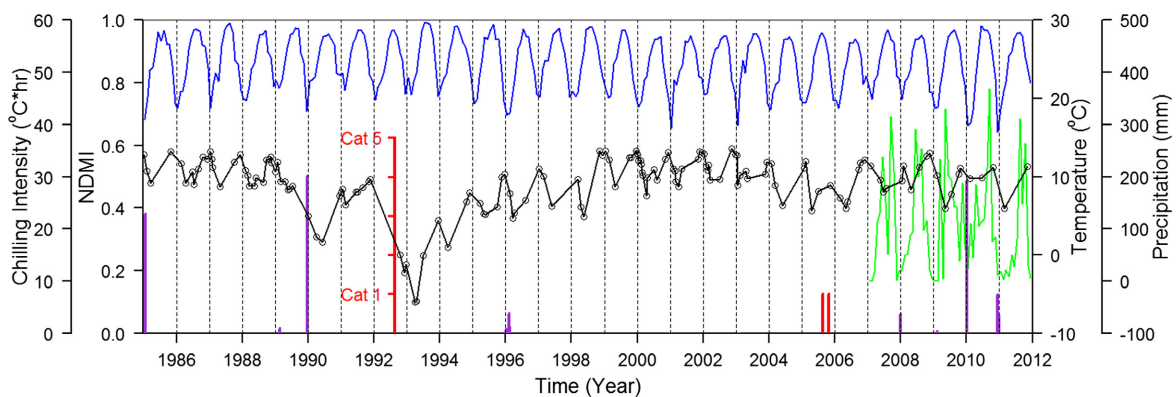


Fig. 10. The mean NDMI (black), monthly averaged temperature (blue), monthly summed precipitation (green), the chilling intensity index calculated by Eq. 10 (purple), and category of hurricanes (red).

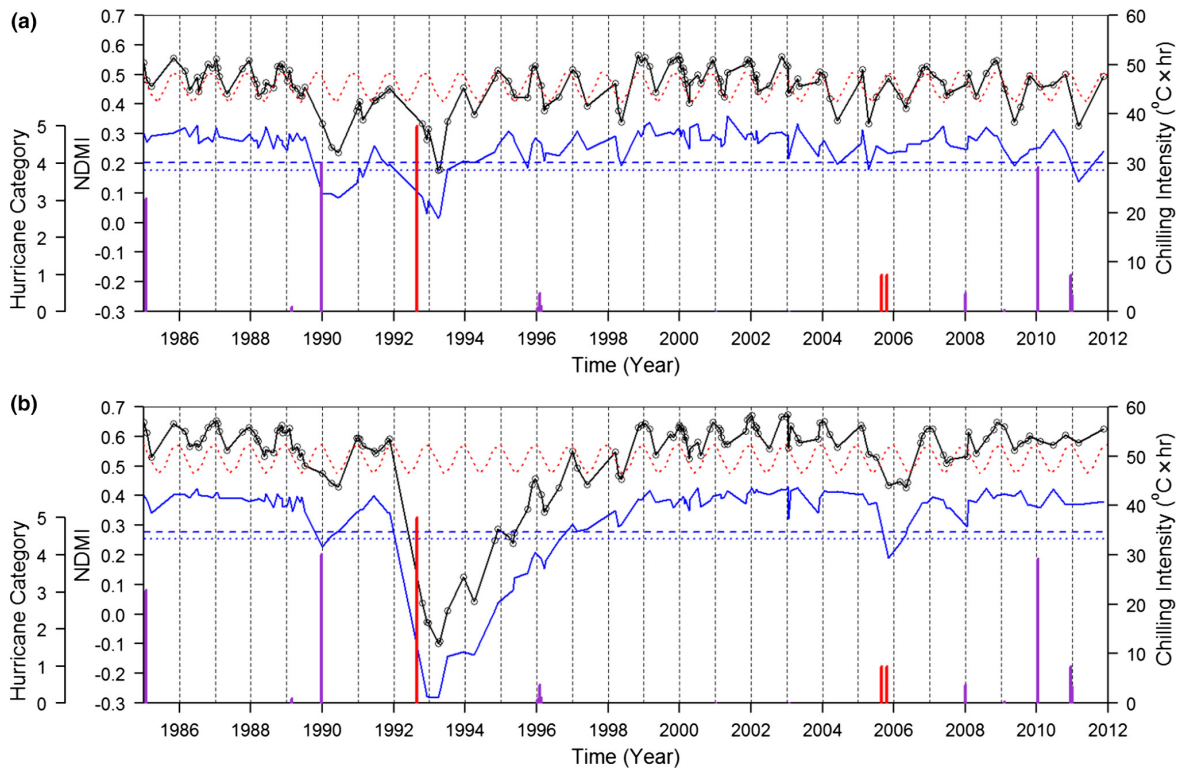


Fig. 11. The mean NDMI of the dwarf and transition mangrove forest (black), seasonal signal (red dashed), the residuals after the seasonal change was removed (blue), $-2 \times$ standard deviation (SD) line (blue dashed), and $-3 \times$ SD line (blue dotted) (a); the mean NDMI of the fringe mangrove forest (black), seasonal signal (red dashed), and the residuals after the seasonal change was removed (blue), $-2 \times$ SD line (blue dashed), and $-3 \times$ SD line (blue dotted) (b). The seasonal change curve has a fixed amplitude and phase. The residual, $-2 \times$ SD, and $-3 \times$ SD curves were offset by a value of 0.2 for the sake of clarity.

values of 0.06 and 0.015, respectively. There was a 1-month phase difference in the seasonal cycles of the dwarf and fringe mangroves. The seasonal change in the fringe mangroves was more regular than in the dwarf forest, resulting in less fluctuating residuals after the seasonal component was removed from the annual mean NDMI. The chilling event of 1989 caused a decrease in the NDMI of the fringe mangroves, but the effects of the other chilling events were small. Hurricane Andrew in 1992 caused the largest decrease of NDMI and it took the mangroves about 6 yr, from March 1993 to December 1998, to recover to the prehurricane value recorded in 1991. As most mangrove trees in the fringe zone were killed by Andrew (Ross et al. 2006), this recovery only meant that the mangrove trees reoccupied the space created by the damage from Andrew, and did not mean that the size of the mangrove trees

recovered to the prehurricane condition. Hurricanes Katrina and Wilma in 2005 caused mild damage in the fringe mangroves, which recovered to the prehurricane condition by December 2006, 1 yr after the hurricanes.

DISCUSSION

Optimal vegetation index

Our analysis of four spectral indices demonstrated that NDMI performed best in detecting seasonal variation and episodic changes induced by chilling events and hurricanes. The basis for the superior performance of NDMI is that NIR (Band 4) reflectance is closely related to vegetation biomass and leaf area index (LAI), and SWIR (Band 5) reflectance is sensitive to plant water content (Boer et al. 2008, Wang et al. 2011, Jensen 2015). Disturbance of mangrove forests

by freezes and hurricanes results in physiological stress, defoliation, or tree death, depending upon the intensity of impacts, altering plant biomass and water content. Reflectance by red mangrove (*Rhizophora mangle*) leaves subjected to stress in a laboratory setting increased in most spectra, but reflectance in SWIR increased much more than reflectance in the red band (Wang and Sousa 2009). Thus, differences in NDMI between healthy and stressed red mangrove leaves are typically larger than differences in NDVI. As red mangrove is the dominant species in the study area (Ross et al. 2006, 2009), it is not unexpected that NDMI outperformed NDVI in tracking the health of mangrove leaves. Another factor that makes NDMI superior to NDVI, especially in context of the dwarf forest, is that NDMI reduces the effect of noise from wet soil on the vegetation signal (Hardisky et al. 1984). Due to the low vegetation density in the dwarf forest (Fig. 2c), more of the soil surface is exposed to the Landsat sensors than in the fringe mangroves. Vegetation coverage in extensive portions of the dwarf forest is less than 40%, while it exceeds 80% in the fringe forest. The fringe forest is often flooded by tidal water. The dwarf forest is less frequently flooded than the fringe, but once inundated by tides or heavy rains, the surface may remain under water for many days (Ross et al. 2006). When dwarf forest soils are covered by a thin layer of water, SWIR reflectance from the soil decreases greatly due to strong absorption by the water, leaving only the reflectance from the vegetation in NDMI (Hardisky et al. 1984). In contrast, reflectance of the red band in NDVI is not diminished as much by water as SWIR reflectance, decreasing the effectiveness of this index in reducing noise from the nonvegetated soil surface.

The other limitation of NDVI is its saturation in dense forests with high LAI (Huete 1988, Gao 1996). NDVI is very responsive under low-biomass conditions, while changing little when biomass is high, especially when NDVI values exceed 0.8. The highest NDVI values in the densely vegetated fringe forest are usually observed when LAI is high in November and December. For example, in November 1988 more than 90% of the NDVI values in the fringe forest were above 0.8, limiting the capacity of the index to reflect vegetation change in this zone. In contrast, few

NDMI values in the fringe forest were larger than 0.8. SAVI and EVI incorporate variation of atmospheric and soil conditions to reduce the saturation and background noise that limit NDVI. However, the coefficients related to atmospheric and soil conditions in Eqs. 2 and 3 are set to be constants. The reflectance from soil in the dwarf forest varies with changing water content as tidal and freshwater flood waters advance and recede. Thus, the constant coefficients do not adequately represent a spatially and temporally variable soil factor, and likely underlie the lower performance of SAVI and EVI in detecting mangrove changes. As in this study, remote sensing of insect defoliation (Townsend et al. 2012) and hurricane damage (Wang et al. 2010) in other forest types also found that NDMI performed better than NDVI in evaluating disturbance. Therefore, it can be concluded that NDMI has an advantage over NDVI and closely related indices in detecting disturbances to mangroves from chilling and hurricane events.

Difference in response of dwarf and fringe forests to chilling and hurricane impacts

Our analysis showed that severe disturbance from hurricanes and chilling events affected the study area's two major ecosystems idiosyncratically, in a pattern that appeared closely related to their respective canopy heights and positions in the landscape. Severe damage from the 1989 chilling event was concentrated in the dwarf forest (Fig. 7d). We speculate that the canopy structure in this ecosystem plays a role during chilling events by altering the microclimate. During the day, sunlight directly penetrates into the forest due to lower tree coverage in the dwarf zone. During the night and morning, the canopy depression occupied by dwarf mangroves, surrounded by fringe mangroves or tall forest occupying the levees along canals and ditches, creates a topographic pocket where cold air settles (Ross et al. 2009). In contrast, the fringe forest's proximity to the ocean and more frequent inundation by warm waters moderate cold temperatures. As a result, a sharper temperature gradient occurs between day and night in the dwarf than in fringe mangroves. Measurements in the study site showed that nighttime temperatures in the dwarf forest were 2–5°C lower than those in

fringe forest when a cold front passed through in December 2003 (Ross et al. 2009). This probably explains why severe damage from chilling events is concentrated in the dwarf mangrove zone.

During an intensive hurricane event such as Andrew, the fringe mangroves suffer severe damage because the trees directly face the forces of high winds and large storm surges, but these forces decay as they move inland. Field surveys in the fringe mangroves after the hurricane showed that high winds broke and uprooted tall trees in the fringe forest, resulting in tree mortality of more than 90% (Ross et al. 2006). In contrast, damage in the dwarf forest was mild for several reasons. First, the vertical wind velocity profile close to the Earth surface during a hurricane approximately follows a logarithmic form (Powell et al. 2003). Because of this boundary layer effect, wind speeds in Hurricane Andrew were greatly reduced as elevation dropped from 8–16 m to 2 m, corresponding to fringe and dwarf canopy heights, respectively. Moreover, the stress due to winds that cause tree damage is proportional to the square of the wind speed, further reducing the effect on dwarf trees in comparison to fringe trees. Second, Ross et al. (2006) speculated that most dwarf mangrove trees may have been immersed by storm water during the peak wind period and thus sheltered from wind action. Based on calibrated numerical modeling of storm surges from Andrew (Zhang et al. 2013), the maximum inundation depths reached about 2–4 m in the dwarf mangrove zone (Fig. 2d), which confirm those speculations. Craighead (1971) also reported that mangrove trees with heights less than 2 m did not suffer complete defoliation during Hurricane Donna in 1960 due to immersion by storm surges. Third, the wind resistance provided by the taller mangrove forest close to the coast may have provided some shelter for the dwarf mangroves further inland. The impact of weak hurricanes such as Katrina and Wilma in 2005 on the dwarf forest was not identifiable through NDMI, while mild damage, mainly defoliation, occurred in the fringe forest.

Seasonal vs. episodic changes

Our analysis indicated that the mangrove forest exhibited a pattern of temporal change that combined regular seasonal fluctuations with

episodic disturbances from hurricanes and chilling events. There is a body of literature on the reproductive and vegetative phenology of mangroves (Duke 1990, Clarke 1994, Kamruzzaman et al. 2013), but studies of seasonal change in leaf area or function focused at whole forests within heterogeneous landscapes have not been previously reported. This vegetation response was tracked by NDMI, an index that is closely correlated with foliar biomass, which is itself the product of leaf area index (LAI) and leaf dry matter content (Wang et al. 2011). The driving force for the seasonal change in NDMI has not yet been identified in mangroves. We speculate that seasonal variation in temperature and precipitation are the main factors causing the intra-annual fluctuations in LAI that we observed. NDMI usually reaches its lowest value in May and starts to increase as temperature rises and the wet season begins (Fig. 10). Temperature and precipitation reach their peaks in August and September, but NDMI continues to increase until December. In January, as temperature reaches the annual minimum, accompanied by diminished precipitation, NDMI shifts into a decreasing mode until May–June. This indicates that leaf area continues to decrease or leaf stress continues to increase through the late spring, even though temperature and precipitation start to increase. There is a large phase difference between seasonal changes of temperature, precipitation, and NDMI. The cause of the seasonal change can only be examined through future field observations. The 1-month phase difference between seasonal changes in dwarf-transition and fringe zones should also be investigated further.

The lag in the mangrove response to the variation in environmental factors is seen not only in the seasonal change of NDMI but also in the response to disturbances. The decrease of NDMI after the severe 1989 chilling event and following the intense 1992 hurricane continued for 4–7 months to April of the following year. Similar to our result based on NDMI change, a field study conducted by Lugo and Patterson-Zucca (1977) documented that damage appeared to be more severe in early April than in February following a January 1977 freeze event in Sea Horse Key, Florida. The recovery processes from chilling events and hurricanes are also different. It

took about 2 yr for NDMI in the mangrove forest to recover to pre-event levels after the severe 1989 chilling event, and about 6 yr for NDMI to recover after Hurricane Andrew. Therefore, temporal resolution is important in capturing a complete picture of the disturbance and recovery process. For example, to detect changes caused by chilling events that usually occur in the December–February period in South Florida, images immediately preceding and several months following the events are required to derive the full magnitude of the disturbance, and subsequent sequential imagery are needed to assess recovery.

The seasonal cycle of NDMI complicates detection of the disturbance signature in satellite images. Only severe disturbances from intense chilling events such as those in 1989 can be detected from the images (Fig. 11). Disturbances from weak chilling events in 1996 and 2001 could not be separated reliably from the seasonal change, even though field surveys demonstrated that these mild chilling events did have significant local and long-lasting ecological impacts in the dwarf forest (Ross et al. 2009). The reason for not detecting these localized effects lies in our approach, which was to use area-wide mean NDMI to establish patterns of change throughout the study area, as well as temporal deviations from these patterns. A natural next step is to evaluate location-specific time series and to develop methods that detect local deviation patterns from inter-annual background and seasonal variations.

Based on the temperature record from the Homestead AFB station (Table 1), three intensive chilling events occurred between 1985 and 2011. The consequence of 1985 chilling event cannot be traced reliably because cloud-free pre-event satellite images are not available. The 1989 chilling event consisted of two instances of low temperature. The first one in February, with a chilling intensity of 1°C h, did not alter the regular trajectory of seasonal change. It was the low temperature event of December 24 and 25, with a chilling intensity of 30°C h, that caused severe damage. Through a comparison of satellite images in December 1988 and April 1990, we found that the severe damage caused by the December 1989 event occurred not only in the study site but also across vast areas of mangroves in Everglades National Park, including along the Florida Gulf coast. Severe and extensive impacts of this chilling event

on citrus trees in inland areas have also been reported (Miller and Downton 1993). In 2010, three low temperature events occurred: one on January 10 and 11, with a chilling intensity of 29°C h; one on December 14 and 15, with a chilling intensity of 7°C h; and one on December 28, with a chilling intensity of 3.2°C h. Although the chilling intensity of the January event was almost as large as that of December 1989, the cumulative impacts of the three 2010 events did not cause as severe damage in the dwarf and transition forests as the earlier one (Fig. 11a). The full magnitude of the January 2010 event could not be quantified because images of March and April were largely obscured by cloud; however, signs of severe damage in the study were not visible in the Landsat TM image from February 2010. On the other hand, this image showed that the mangroves along the south Florida Gulf coast experienced severe damage. Anomalous tidal water levels or wind speeds were not observed during the January 2010 event, therefore, the specific reasons for the weak response of mangroves are not clear and deserve further investigation. In contrast, severe damage was detected in the dwarf and transition forests after the two low temperature events in December 2010, though the chilling intensities of these events were relatively small. The consecutive occurrence of two weak low temperature events may explain the severe damage in the dwarf and transition forests indicated by the image of February 2011. It is also possible that despite not causing immediate damage in the dwarf and transition forests, the low temperatures of January 2010 caused trees to be more vulnerable to the events of the following winter.

Implications of disturbances to forest change

Hurricanes, chilling events, and lightning strikes can cause high local mortality among mangroves (Lugo and Patterson-Zucca 1977, Smith et al. 1994, Stevens et al. 2006, Zhang et al. 2008), while creating spatial heterogeneity at different landscape scales. Canopy-replacing levels of damage are frequently observed over large areas in which hurricane winds and storm surges are highest (Baldwin et al. 1995, Sherman et al. 2001, Ross et al. 2006), but the damage decreases away from the storm's path and away from the shoreline as the energy of wind and storm surge decay. For example, during

Hurricane Andrew severe forest damage was restricted to within the 40- to 50-km wide hurricane eye wall (Doyle et al. 1995). Freezes in subtropical mangrove ecosystems are intermediate-to-large scale disturbances, depending upon the intensity and extent of the event, forming patches of severe damage in interior mangrove forests while leaving forests next to the ocean untouched. In contrast, lightning strikes often generate small scale damage pockets of 10–20 m in diameter (Zhang et al. 2008). These disturbances, occurring at different scales and in different zones, have profound effects on the community dynamics of the mangrove forest.

Both fringe and dwarf forests of the study area comprise a complex mosaic of four mangroves, though red mangrove is by far the most abundant species. Within this landscape, chilling disturbances play an especially important role in maintaining species abundance and community structure in the dwarf mangrove forest. Ross et al. (2009) showed that high mortality of red mangroves from a 1996 chilling event provided an opportunity for the development of white mangrove as well as buttonwood. The repetitive occurrence of severe chilling events in the dwarf forest results in heterogeneity within the landscape by converting community composition dominated by red mangroves to one with a mixture of red, white, and black mangrove, as well as buttonwood. The large open conditions caused by severe hurricane damage also provide opportunities for regeneration of all of the mangrove species, especially the shade intolerant white mangrove (Zhang et al. 2008). As the climate changes in the future, fewer chilling events are expected due to the increase in global temperature (Ross et al. 2009), and a decrease in the total number of hurricanes but an increase in intense ones such as Andrew (Knutson et al. 2010) are also anticipated. Such changes are likely to alter the regulation function associated with disturbances from chilling events and hurricanes. It is difficult to predict the future trajectory of the mangrove forest in the study area because the heterogeneity created by a single hurricane and freeze is multiplied over time, forming a spatio-temporal tapestry (Brokaw 2012) wherein each patch modifies subsequent disturbances, while being itself altered by them. However, the overall trend with respect to disturbance seems to favor

an increase in red mangrove in a less heterogeneous dwarf forest, linked in the landscape with a more heterogeneous fringe forest.

CONCLUSION

The spatial and temporal changes of the mangrove forests were analyzed by using a time series of 150 Landsat TM images spanning 27 yr in combination with LiDAR data collected in 2007. Vegetation indices including NDVI, SAVI, EVI, and NDMI were employed to quantify changes in the mangrove forest. Our analysis of the distribution of vegetation index difference values demonstrated that NDMI was the optimal index for identifying changes induced by seasonal factors, chilling events, and hurricanes. NDMI was more sensitive to the defoliation, damage, and death of mangrove trees than NDVI, SAVI, and EVI because the NIR band was responsive to changes in biomass and LAI, and SWIR was responsive to the water content in trees. There were distinct spatial patterns in response to disturbances from chilling events and hurricanes, and these were related to the canopy height gradient. The most severe damage from chilling events were concentrated in interior dwarf and transition mangrove forests with tree heights less than 4 m, because of lower temperatures due to accumulation of cold air in canopy depressions. In contrast, fringe mangrove forests with tree heights above 4 m suffered most damage from hurricanes because trees were exposed to the highest winds and largest storm surges.

There was no significant long-term trend in the vegetation changes represented by NDMI; however, a seasonal change characterized the dwarf, transition, and fringe mangrove forests, presumably regulated by seasonal changes in temperature and precipitation. Periodicity in NDMI in the fringe forest lagged 1 month behind that observed in the dwarf and transition forests. There were also lags in damage to trees in response to the impact of chilling events and hurricanes; it took the mangroves about 4–7 months to reach a low point in vegetation condition after intensive chilling and hurricane events. Therefore, cloud-free optical satellite images immediately before the events, e.g., in November or December for chilling events, and 2–7 months

after the events, e.g., March–May are required to capture the full damage extent of the disturbances. The recovery time of NDMI from these disturbances was 2 and 6 yr for chilling and hurricane events, respectively.

A decrease in the occurrence of chilling events and an increase in intense hurricanes in response to future global climate changes will probably result in a reduction of local heterogeneity in the dwarf forest and an increase in heterogeneity in the fringe forest. The vegetation index-based remote sensing method provides an effective and simple way to monitor changes in mangrove forests at a scale difficult to attain from the ground alone. In combination with targeted field observations, the baseline that we established using a time series of Landsat images will be useful for disentangling seasonal, episodic, and long-term changes in the mangrove forests, and thereby helping to detect the signal of future climate changes.

ACKNOWLEDGMENTS

We thank anonymous reviewers for valuable comments and suggestions. This research was enhanced by collaborations with the Florida Coastal Everglades Long-Term Ecological Research Program (funded by the National Science Foundation, DBI-0620409). This is contribution #791 from the Southeast Environmental Research Center at Florida International University.

LITERATURE CITED

- Baldwin, A. H., W. J. Platt, K. L. Gathen, J. M. Lessmann, and T. J. Rauch. 1995. Hurricane damage and regeneration in fringe mangrove forests of southeast Florida, USA. *Journal of Coastal Research* 21:169–183.
- Boer, M. M., C. Macfarlane, J. Norris, R. J. Sadler, J. Wallace, and P. F. Grierson. 2008. Mapping burned areas and burn severity patterns in SW Australian eucalypt forest using remotely-sensed changes in leaf area index. *Remote Sensing of Environment* 112:4358–4369.
- Brokaw, N. 2012. *A Caribbean forest tapestry: the multidimensional nature of disturbance and response*. Oxford University Press, New York, New York, USA.
- Cavanaugh, K. C., J. R. Kellner, A. J. Forde, D. S. Gruner, J. D. Parker, W. Rodriguez, and I. C. Feller. 2014. Poleward expansion of mangroves is a threshold response to decreased frequency of extreme cold events. *Proceedings of the National Academy of Sciences* 111:723–727.
- Clarke, P. J. 1994. Base-line studies of temperate mangrove growth and reproduction; demographic and litterfall measures of leafing and flowering. *Australian Journal of Botany* 42:37–48.
- Craighead, F. C. 1971. *The trees of south Florida*. University of Miami Press Coral Gables, Miami, Florida, USA.
- Davis, J. C. 2002. *Statistics and data analysis in geology*, Third edition. Wiley, New York, New York, USA.
- Doyle, T. W., T. J. Smith III, and M. B. Robblee. 1995. Wind damage effects of Hurricane Andrew on mangrove communities along the southwest coast of Florida, USA. *Journal of Coastal Research* 21:159–168.
- Duke, N. 1990. Phenological trends with latitude in the mangrove tree *Avicennia marina*. *Journal of Ecology* 78:113–133.
- Ellis, P. D. 2010. *The essential guide to effect sizes: Statistical power, meta-analysis, and the interpretation of research results*. Cambridge University Press, New York, New York, USA.
- Gao, B.-C. 1996. NDWI—a normalized difference water index for remote sensing of vegetation liquid water from space. *Remote Sensing of Environment* 58:257–266.
- Giri, C., E. Ochieng, L. L. Tieszen, Z. Zhu, A. Singh, T. Loveland, J. Masek, and N. Duke. 2011. Status and distribution of mangrove forests of the world using earth observation satellite data. *Global Ecology and Biogeography* 20:154–159.
- Hardisky, M. A., F. C. Daiber, C. T. Roman, and V. Klemas. 1984. Remote sensing of biomass and annual net aerial primary productivity of a salt marsh. *Remote Sensing of Environment* 16:91–106.
- Huete, A. R. 1988. A soil-adjusted vegetation index (SAVI). *Remote Sensing of Environment* 25:295–309.
- Huete, A., C. Justice, and H. Liu. 1994. Development of vegetation and soil indices for MODIS-EOS. *Remote Sensing of Environment* 49:224–234.
- Huete, A., H. Liu, K. Batchily, and W. Van Leeuwen. 1997. A comparison of vegetation indices over a global set of TM images for EOS-MODIS. *Remote Sensing of Environment* 59:440–451.
- Huete, A., K. Didan, T. Miura, E. P. Rodriguez, X. Gao, and L. G. Ferreira. 2002. Overview of the radiometric and biophysical performance of the MODIS vegetation indices. *Remote Sensing of Environment* 83:195–213.
- 3001 Inc. 2008. *Vertical Accuracy Report: Block 1*. Page 81, Slidell, Louisiana, USA.

- Jensen, J. R. 2015. Introductory digital image processing: a remote sensing perspective. Fourth edition. Pearson Education Inc., New York, New York, USA.
- Kamruzzaman, M., S. Sharma, and A. Hagihara. 2013. Vegetative and reproductive phenology of the mangrove *Kandelia obovata*. *Plant Species Biology* 28:118–129.
- Knutson, T. R., J. L. McBride, J. Chan, K. Emanuel, G. Holland, C. Landsea, I. Held, J. P. Kossin, A. Srivastava, and M. Sugi. 2010. Tropical cyclones and climate change. *Nature Geoscience* 3:157–163.
- Krauss, K. W., K. L. McKee, C. E. Lovelock, D. R. Cahoon, N. Saintilan, R. Reef, and L. Chen. 2014. How mangrove forests adjust to rising sea level. *New Phytologist* 202:19–34.
- Kuenzer, C., A. Bluemel, S. Gebhardt, T. V. Quoc, and S. Dech. 2011. Remote sensing of mangrove ecosystems: A review. *Remote Sensing* 3:878–928.
- Lagomasino, D., R. M. Price, D. Whitman, P. K. Campbell, and A. Melesse. 2014. Estimating major ion and nutrient concentrations in mangrove estuaries in Everglades National Park using leaf and satellite reflectance. *Remote Sensing of Environment* 154:202–218.
- Lugo, A. E., and C. Patterson-Zucca. 1977. The impact of low temperature stress on mangrove structure and growth. *Tropical Ecology* 18:149–161.
- Lugo, A. E., and S. C. Snedaker. 1974. The ecology of mangroves. *Annual Review of Ecology and Systematics* 5:39–64.
- Masek, J. G., E. F. Vermote, N. E. Saleous, R. Wolfe, F. G. Hall, K. F. Huemmrich, F. Gao, J. Kutler, and T.-K. Lim. 2006. A Landsat surface reflectance dataset for North America, 1990–2000. *Geoscience and Remote Sensing Letters, IEEE* 3:68–72.
- Masek, J. G., C. Huang, R. Wolfe, W. Cohen, F. Hall, J. Kutler, and P. Nelson. 2008. North American forest disturbance mapped from a decadal Landsat record. *Remote Sensing of Environment* 112:2914–2926.
- Miller, K. A., and M. W. Downton. 1993. The freeze risk to Florida citrus. Part 1: Investment decisions. *Journal of Climate* 6:354–363.
- Negrón-Juárez, R., D. B. Baker, J. Q. Chambers, G. C. Hurtt, and S. Goosem. 2014. Multi-scale sensitivity of Landsat and MODIS to forest disturbance associated with tropical cyclones. *Remote Sensing of Environment* 140:679–689.
- Olmsted, I., H. Dunevitz, and W. Platt. 1993. Effects of freezes on tropical trees in Everglades National Park Florida, USA. *Tropical Ecology* 34:17–34.
- Powell, M. D., and S. H. Houston. 1996. Hurricane Andrew's landfall in south Florida. Part II: Surface wind fields and potential real-time applications. *Weather and Forecasting* 11:329–349.
- Powell, M. D., P. J. Vickery, and T. A. Reinhold. 2003. Reduced drag coefficient for high wind speeds in tropical cyclones. *Nature* 422:279–283.
- Pugh, D. T. 1996. Tides, surges and mean sea-level (reprinted with corrections). John Wiley & Sons Ltd., Chichester, UK.
- Ross, M., J. Meeder, J. Sah, P. Ruiz, and G. Telesnicki. 2000. The southeast saline Everglades revisited: 50 years of coastal vegetation change. *Journal of Vegetation Science* 11:101–112.
- Ross, M. S., P. L. Ruiz, G. J. Telesnicki, and J. F. Meeder. 2001. Estimating above-ground biomass and production in mangrove communities of Biscayne National Park, Florida (USA). *Wetlands Ecology and Management* 9:27–37.
- Ross, M. S., P. L. Ruiz, J. P. Sah, D. L. Reed, J. Walters, and J. F. Meeder. 2006. Early post-hurricane stand development in fringe mangrove forests of contrasting productivity. *Plant Ecology* 185:283–297.
- Ross, M. S., P. L. Ruiz, J. P. Sah, and E. J. Hanan. 2009. Chilling damage in a changing climate in coastal landscapes of the subtropical zone: a case study from south Florida. *Global Change Biology* 15:1817–1832.
- Ruiz, P., M. Ross, J. Walters, B. Hwang, E. Gaiser, and F. Tobias. 2002. L-31E wetland and flow monitoring (SFWMD Contract C-12409): Vegetation of coastal wetlands in Biscayne National Park: Blocks 6–8. Florida International University, Miami, Florida, USA.
- Ruiz, P., P. Houle, and M. Ross. 2008. The terrestrial vegetation of Biscayne National Park, FL, USA derived from aerial photography, NDVI, and LiDAR. Florida International University, Miami, Florida, USA.
- Saintilan, N., N. C. Wilson, K. Rogers, A. Rajkaran, and K. W. Krauss. 2014. Mangrove expansion and salt marsh decline at mangrove poleward limits. *Global Change Biology* 20:147–157.
- Sherman, R. E., T. J. Fahey, and P. Martinez. 2001. Hurricane impacts on a mangrove forest in the Dominican Republic: Damage patterns and early recovery. *Biotropica* 33:393–408.
- Smith, T. J., M. B. Robblee, H. R. Wanless, and T. W. Doyle. 1994. Mangroves, hurricanes, and lightning strikes. *BioScience* 44:256–262.
- Spalding, M. D., A. L. McIvor, M. W. Beck, E. W. Koch, I. Möller, D. J. Reed, P. Rubinoff, T. Spencer, T. J. Tolhurst, and T. V. Wamsley. 2014. Coastal ecosystems: a critical element of risk reduction. *Conservation Letters* 7:293–301.
- Stevens, P. W., S. L. Fox, and C. L. Montague. 2006. The interplay between mangroves and saltmarshes at the transition between temperate and subtropical climate in Florida. *Wetlands Ecology and Management* 14:435–444.
- Thapa, B. 2014. Spatio-temporal analysis of chilling events in mangrove forests of south Florida. Florida International University, Miami, Florida, USA.
- Townsend, P. A., A. Singh, J. R. Foster, N. J. Rehberg, C. C. Kingdon, K. N. Eshleman, and S. W. Seagle. 2012. A general Landsat model to predict canopy

- defoliation in broadleaf deciduous forests. *Remote Sensing of Environment* 119:255–265.
- USGS. 2015. Product Guide: Landsat4-7 Climate Data Record (CDR) Surface Reflectance. U.S. Geological Survey, Reston, Virginia, USA.
- Vermote, E., N. El Saleous, C. Justice, Y. Kaufman, J. Privette, L. Remer, J. Roger and D. Tanre. 1997. Atmospheric correction of visible to middle-infrared EOS-MODIS data over land surfaces: Background, operational algorithm and validation. *Journal of Geophysical Research* 102:17131–17141.
- Wang, L., and W. P. Sousa. 2009. Distinguishing mangrove species with laboratory measurements of hyperspectral leaf reflectance. *International Journal of Remote Sensing* 30:1267–1281.
- Wang, F., and Y. J. Xu. 2010. Comparison of remote sensing change detection techniques for assessing hurricane damage to forests. *Environmental Monitoring and Assessment* 162:311–326.
- Wang, L., W. P. Sousa, P. Gong, and G. S. Biging. 2004. Comparison of IKONOS and QuickBird images for mapping mangrove species on the Caribbean coast of Panama. *Remote Sensing of Environment* 91:432–440.
- Wang, W., J. J. Qu, X. Hao, Y. Liu, and J. A. Stanturf. 2010. Post-hurricane forest damage assessment using satellite remote sensing. *Agricultural and Forest Meteorology* 150:122–132.
- Wang, L., E. R. Hunt, J. J. Qu, X. Hao, and C. S. Daughtry. 2011. Towards estimation of canopy foliar biomass with spectral reflectance measurements. *Remote Sensing of Environment* 115:836–840.
- White, P. S., and A. Jentsch. 2001. The search for generality in studies of disturbance and ecosystem dynamics. *Progress in Botany* 62:399–450.
- Wilson, E. H., and S. A. Sader. 2002. Detection of forest harvest type using multiple dates of Landsat TM imagery. *Remote Sensing of Environment* 80:385–396.
- Zhang, K. 2008. Identification of gaps in mangrove forests with airborne LIDAR. *Remote Sensing of Environment* 112:2309–2325.
- Zhang, K., B. C. Douglas, and S. P. Leatherman. 2000. Twentieth-century storm activity along the US east coast. *Journal of Climate* 13:1748–1761.
- Zhang, K., M. Simard, M. Ross, V. H. Rivera-Monroy, P. Houle, P. Ruiz, R. R. Twilley, and K. Whelan. 2008. Airborne laser scanning quantification of disturbances from hurricanes and lightning strikes to mangrove forests in Everglades National Park, USA. *Sensors* 8:2262–2292.
- Zhang, K., Y. Li, H. Liu, J. Rhome, and C. Forbes. 2013. Transition of the coastal and estuarine storm tide model to an operational storm surge forecast model: A case study of the Florida coast. *Weather and Forecasting* 28:1019–1037.
- Zhu, Z., C. E. Woodcock, and P. Olofsson. 2012. Continuous monitoring of forest disturbance using all available Landsat imagery. *Remote Sensing of Environment* 122:75–91.